Array Mode Analysis of Two-Dimensional Phased Arrays of Vertical Cavity Surface Emitting Lasers

HOI-JUN YOO, J. R. HAYES, MEMBER, IEEE, EUNG GI PAEK, A. SCHERER, AND YOUNG-SE KWON

Abstract—**We have investigated the modal properties of two-dimensional phase-locked arrays of vertical cavity surface emitting lasers where the spatial coherency across the aperture comes from the evanescent coupling of the optical fields of the lasers. Typical two-dimensional arrays can be separated into three categories: the periodic array, the circular array, and the centered polygonal array (or concentric circular array). The circular array and centered polygonal array support a more circular symmetric output beam than the periodic array which is a simple two-dimensional extension of a linear array. The far-field pattern of the two-dimensional array has an azimuthal angle dependence such that near zenith, the fundamental array mode shows a single-lobe beam but with increasing angle many sidelobes appear. The highest array mode has a double-lobed far-field pattern near zenith, as in the case of the linear array. The centered polygonal array shows the most circularly symmetric beam pattern of the three which can be controlled by varying the excitation amplitude of the center laser. We have shown that symmetry plays an important role in determining the array mode and that the use of VCSE lasers give a good longitudinal mode selection leading to dynamic single-mode operation. These results can be extended to a quantum box laser array to give better optical beam control.**

I. INTRODUCTION

THE technology for fabricating laser arrays has continued to progress such that output powers as high as several watts CW can be easily obtained. This can lead to many applications such as laser printers, optical recorders, solid-state laser pumps and space communication, where very high output power, high-energy conversion efficiency, and good output beam quality are required [1], [2]. The output power emitted from a lasing source is proportional to the area occupied by the lasing mode. In order to increase the aperture area one approach has been to fabricate linear arrays of closely spaced narrow-stripe lasers and use the evanescent coupling between lasers to bring coherency across the array aperture. However, simple linear integration of the lasers leads to a long array that limits the possible output power and packing density. More recently, other approaches have been used to enlarge the area of the aperture using two-dimensional integration of surface emitting lasers [3]–[7] or vertical stacking of linear arrays of conventional edge emitting lasers [8].

Manuscript received October 11, 1989; revised January 4, 1990.

H.-J. Yoo is with Bellcore, Red Bank, NJ 07701, on leave from the Department of Electrical Engineering, Korea Advanced Institute of Science and Technology, Seoul, Korea.

J. R. Hayes, E. G. Paek, and A. Scherer are with Bellcore, Red Bank, NJ 07701.

Y.-S. Kwon is with the Department of Electrical Engineering, Korea Advanced Institute of Science and Technology, Seoul, Korea.

IEEE Log Number 9035221.

For the implementation of a monolithic two-dimensional array, most research has focused on the use of conventional "horizontal cavity" laser that has a surface grating [3] or 45°-beam deflector [4]–[6] to couple the light out vertically. In these cases, the output beam has several one dimensional phased arrays separated by a few tens to several hundreds of microns from each other. Therefore, they cannot lock the phases of each array due to their large separation that clearly reduces their packing density. Also, a few attempts have been directed toward obtaining an incoherent array (not phase locked) using vertical cavity lasers [7], [9]. Very recently, the authors have demonstrated the first phase locked two-dimensional array of vertical cavity surface emitting lasers [10].

In this paper, we examine a two-dimensional phase-locked array where the spatial coherency across the array comes from the evanescent coupling of the optical field. Also, we present the analysis of a planar array composed of vertical cavity surface emitting lasers using a coupled mode theory which has been successfully applied to the analysis of linear laser arrays [11]. From the analysis, the allowed modes, "array modes," of a phase locked two-dimensional array of different structures with weak coupling can be obtained. The near- and far-field pattern of the array modes can be derived analytically. In addition, we can solve the splitting of the oscillation frequency of the array modes from that of the individual emitters as a function of the coupling coefficient.

A vertical cavity surface emitting (VCSE) laser diode comprises a small volume active region and vertically stacked layers which form mirrors that are intrinsically easy to integrate into a closely packed two-dimensional laser array [12]. There are many advantages of two-dimensional phase locked arrays. The first advantage is their high-power capability. This occurs because the active area can be widened more than that of a linear array. Another advantage is its improved directionality. The directionality of the array depends on the emitting area of the laser and hence, a greater degree of directionality can be obtained from a two-dimensional array. Also, there is greater flexibility in the geometry of array structures in two dimensions suggesting that the shape of the output beam can be better controlled to conform to the pattern which a specific application requires. In addition, we can extend the well-developed principles of microwave phased array antenna theory into the optical region as well. In the following, we analyze the coupling characteristics between two

VCSE lasers. Based on this analysis, we will extend the theory to two-dimensional coupled laser arrays.

II. Coupling Between VCSE Lasers

The vertical cavity surface emitting laser (VCSE laser) [12]–[16] which will be analyzed in this paper, has the same structure as that reported by Jewell *et al.* [13]. As shown in Fig. 1, it consists of multiple quarter wavelength AlAs–GaAs stacking layers that form a high reflectance distributed Bragg reflector (DBR), an $Al_{0.5}Ga_{0.5}As$ cavity layer of half wavelength thickness, and an 80 A–100 A thick InGaAs strained quantum well active region. The p-electrode is evaporated on the top of the cylindrical post which is etched by chemical ion beam etching, and the n-electrode is put on the backside of the n^+ GaAs wafer. When sufficient bias is applied, lasing occurs and a laser beam of 1 μm wavelength emerges from the bottom of the substrate, since GaAs is transparent to the emitting wavelength. Usually, the laser has a cylindrical shape to reduce the surface recombination current along the exposed sidewall.

If the electron density along the active region is uniform, we can approximate the laser structure as a cylindrical dielectric waveguide. To determine the characteristics of light propagation in a dielectric cylinder, Maxwell's equations must be solved in the cylinder and the cladding, subject to the boundary conditions that the tangential components of the electric and magnetic field vectors E and H must be continuous across the boundary. Using the cylindrical coordinates r and θ, the solution of the Maxwell equation is given as Bessel functions [17]. In the laser, the ordinary Bessel function is chosen and in the cladding the modified Hankel function is chosen. From the solutions of the eigenvalue equation, which can be obtained by imposing the boundary conditions, the single transverse mode condition of the laser can be obtained [17].

The coupling coefficient between two VCSE lasers is given as the overlap integral of the E-field within the laser and E-field from the other laser. However, the explicit expression of the coupling coefficient between two VCSE lasers is complicated [19] and numerical solutions are shown in Fig. 2. Fig. 2 shows the product of coupling coefficient c and the radius of a laser a as a function of d/a. In calculating Fig. 2, we assumed that each laser supports the fundamental mode HE_{11}. Although the single-mode condition is not satisfied, this assumption is still effective. Because the TE_{01}, TM_{01}, and HE_{21} modes have nearly the same propagation constants, coupling between all three modes is possible. Linear combination of these three modes can be found that lead to linearly polarized modes. However, coupling between these modes are not stable throughout the round trip in the laser cavity due to their finite difference in propagation constants.

It can clearly be seen from Fig. 2 that a larger coupling coefficient can be obtained due to the further penetration of the field into the cladding with a decrease of laser radius. In the linear array, the coupling coefficient between

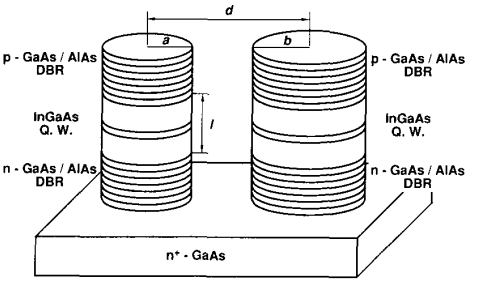

Fig. 1. Schematic diagram of two closely spaced vertical cavity surface emitting lasers that are discussed in this paper.

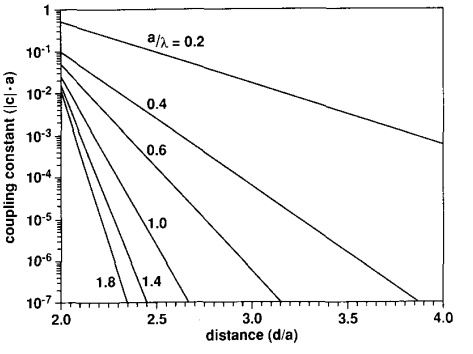

Fig. 2. Product of coupling coefficient, $|c|$ and radius of laser, between two identical vertical cavity surface emitting lasers with air cladding as function of d/a.

lasers is of the order 10^{-3}-10^{-4} [20]. If we choose a coupling coefficient of 10^{-3}, the distance between two 1 μm radius lasers has to be less than 0.2 μm for coupling. This critical distance can be increased by regrowth of an AlGaAs buried layer [18]. In this case, the small difference of refractive index between the laser and cladding regions alleviates the critical design constraint of the laser for single-mode operation as well as the distance between lasers for significant coupling.

III. Two-Dimensional Arrays

As described earlier, the use of a two-dimensional array leads to more freedom in the design of the arrays and in particular the structure of two-dimensional phase locked arrays. In this paper we will analyze three typical array structures, such as a periodic array, a circular array, and a centered polygonal array (or concentric circular array), as shown in Fig. 3. The basic structure of a two-dimensional array is a periodic array in which each element resides on a two-dimensional lattice point [21] to form either a rectangular lattice or a triangular lattice as shown in Fig. 3(a). The circular array in Fig. 3(b) is a unique two-dimensional array [22] and understanding its behavior is helpful for the analysis of concentric circular arrays. The centered polygonal arrays (or concentric circular array) in Fig. 3(c) are of the most practical interest [23]. Since we will be investigating a simple concentric circular array, we can compare the beam patterns of concentric circular

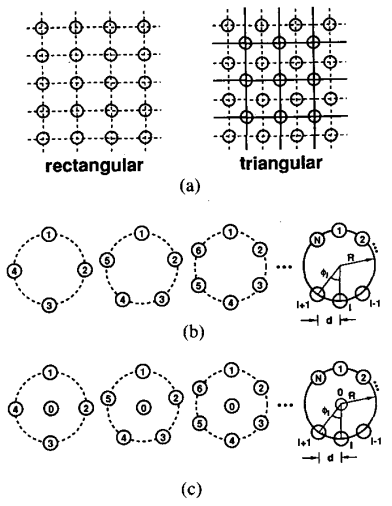

Fig. 3. Three schematics of two-dimensional arrays. (a) Periodic array in which only two arrays are of interest; rectangular and triangular arrays. (b) Circular array, where each element occupies vertex of polygon. (c) Centered polygonal array (or concentric circular array), which is circular array having centered laser.

array with that of the circular array in order to understand the effect of the center laser to the resulting beam patterns. In what follows, we briefly summarize the coupled mode equations of two-dimensional arrays.

If each individual laser waveguide, when isolated from its neighbors, supports a single HE_{11}-like mode [17], the optical mode for a laser of index l and m can be described by its electric field as

$$\psi_{lm} = E_{lm}(r, \theta)e^{i\beta_{lm}z} \tag{1}$$

where $l = 1, 2, \cdots, N_1$ and $m = 1, 2, \cdots, N_2$ and β_{lm} is the complex propagation constant. The total electric field E of the array is given as

$$E = \sum_{l=1}^{N_1}\sum_{m=1}^{N_2} A_{lm}\psi_{lm} = \sum_{l=1}^{N_1}\sum_{m=1}^{N_2} A_{lm}(z)E_{lm}(r, \theta)e^{i\beta_{lm}z} \tag{2}$$

where A_{lm} is a complex coefficient due to the interaction among the array elements.

By substituting (2) into the usual Maxwell equation, we obtain a set of equations for the array modes as

$$\frac{dA_{mn}}{dz} = \sum_{l=1}^{N_1}\sum_{m=1}^{N_2} iC_{lmpq}A_{pq}e^{i(\beta_{pq}-\beta_{lm})z} \tag{3}$$

where C_{lmpq} is a coupling coefficient between A_{lm} and A_{pq}. Assuming only nearest-neighbor coupling, the coupled-mode equations for a two-dimensional array can be solved analytically as shown in the following sections.

The far-field pattern of the array can be obtained by the multiplication of the array factor and elementary envelope field [24]. The array factor of a two-dimensional array is calculated by summing the vector field of each element in the array at each point in space. The detailed analysis depends on the array structures, which will be discussed in following sections.

A. Periodic Array

The periodic array is a two-dimensional extension of the linear array. An ideal periodic array is constructed by the infinite in plane repetition of identical structural units. Generally, there are five Bravais lattices in two dimensions, one oblique lattice and four special lattices satisfying the special point operations [25]. But if we characterize the lattice by the shape of its primitive translation vectors, we can select only two lattices in the two dimensions, rectangular and triangular. In this paper, the analysis of only the rectangular array will be discussed. The triangular array, however, can be considered as the summation of two rectangular subarrays. This is shown in Fig. 3(a) as the superposition of a dashed and a solid lattice. The analysis follows the same mathematics as the rectangular array.

It is assumed that each laser couples to only its four nearest neighbors and A_{lm} has a $e^{i\delta_{lm}}$ dependence. Also, it is assumed that every coupling coefficient between nearest neighbors along the x-direction is the same as C_1 and along the y direction is the same as C_2. Then, the coupled mode equation (3) becomes

$$A_{lm} = C_1(A_{lm+1} + A_{lm-1}) + C_2(A_{l-1m} + A_{l+1m}). \tag{4}$$

δNote that (4) reduces to the coupled mode equation of a linear array if C_1 or C_2 goes to zero. By substituting $A_{lm} = De^{l\eta + m\xi}$ into (4), the eigenvalue is obtained as $\delta = 2C_1 \cos \xi + 2C_2 \cos \eta$ where ξ and η will be determined by the boundary conditions.

If the array has $N_1 \times N_2$ elements as illustrated in Fig. 4, then η and ξ are given as $p\pi/(N_1 + 1)$ and $q\pi/(N_2 + 1)$, respectively, from the boundary conditions that $A_{on} = A_{N_1 n} = 0$ and $A_{mo} = A_{mN_2+1} = 0$, where p and q are integers from 1 to N_1 and N_2, respectively. Therefore, A_{lm}^{pq} is given as

$$A_{lm}^{pq} = \sin\left(\frac{lp\pi}{N_1 + 1}\right) \cdot \sin\left(\frac{mq\pi}{N_2 + 1}\right) \tag{5}$$

and the propagation constant of the p-th $\times$ q-th order array mode as

$$\gamma_{pq} = \beta + C_1 \cos\left(\frac{p\pi}{N_1 + 1}\right) + C_2 \cos\left(\frac{q\pi}{N_2 + 1}\right). \tag{6}$$

The splitting in the propagation constants of the array modes is proportional to the coupling constants C_1 and C_2 as in the case of the linear array [10], [11]. If N_1 and N_2 are very large, the propagation constants of the array modes form a quasi-continuum in the range

$$\beta - 2(C_1 + C_2) < \gamma < \beta + 2(C_1 + C_2). \tag{7}$$

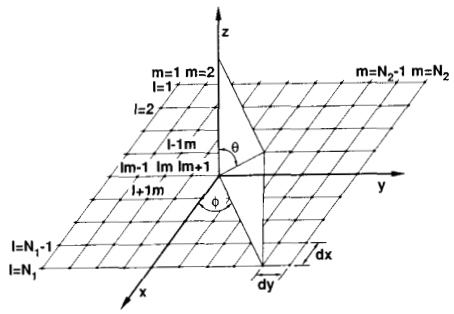

Fig. 4. $N_1 \times N_2$ rectangular array. Distance between lasers along x direction is d_x and distance along y direction is d_y.

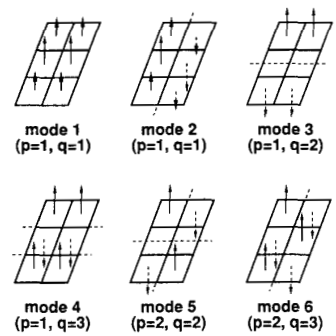

Fig. 5. Schematic illustration of near-field distribution of supermodes of a 2×3 rectangular array.

If $C_1 = C_2 = C$, the maximum wavelength splitting in the longitudinal mode becomes

$$\Delta\lambda = \Delta\gamma \frac{\lambda_0^2}{2\pi n_e} = 8C \frac{\lambda_0^2}{2\pi n_e}. \tag{8}$$

Since the $\Delta\lambda$ of uncoupled lasers is given by $\lambda_0^2/2ln_e$ where l is the cavity length and n_e is the effective refractive index of cavity, the $\Delta\lambda$ of the array modes is smaller than the $\Delta\lambda$ of the uncoupled lasers if $Cl \ll 1$. Because the cavity length of the VCSE laser is very short, this condition is easily satisfied. In addition, the mode splitting between two adjacent array modes will be less than the maximum splitting. Therefore, it may be possible for the array to support multimode oscillation even if an elemental laser has single-mode operation. This may be avoided if we increase the coupling coefficient that will lead to a larger $\Delta\lambda$ between array modes as can be seen from (8).

The array factor of the pth $\times$ qth order array mode is given as

$$AF_{pq}(\theta, \phi) = \sum_{l=1}^{N_1} \sum_{m=1}^{N_2} A_{lm}^{pq} \exp\left[-ik_0 \cdot \sin\theta(ld_x \cos\phi + md_y \sin\phi)\right]. \tag{9}$$

By substituting (5) into (6), we obtain the array factor as the product of two linear array factors that have been calculated by J. K. Butler [10], such as

$$AF_{pq}(\theta, \phi) = \left[\frac{\sin\left[N_1(s + \theta_p)/2\right]}{\sin\left[(s + \theta_p)/2\right]} - (-1)^p \frac{\sin\left[N_1(s - \theta_p)/2\right]}{\sin\left[(s - \theta_p)/2\right]}\right] \times \left[\frac{\sin\left[N_2(t + \theta_q)/2\right]}{\sin\left[(t + \theta_q)/2\right]} - (-1)^q \frac{\sin\left[N_2(t - \theta_q)/2\right]}{\sin\left[(t - \theta_q)/2\right]}\right] \tag{10}$$

where $s = k_0 d_x \sin\theta \cos\phi$, $t = k_0 d_y \sin\theta \sin\phi$, $\theta_p = p\pi/(N_1 + 1)$ and $\theta_q = q\pi/(N_2 + 1)$.

Fig. 5 shows the schematic illustration of the near-field pattern of the array modes of a 2×3 periodic array. Note that the excitation amplitude of the individual lasers is different across the array. The in-phase array mode has a field amplitude distribution peaked in the middle region of the array. Therefore, for uniform current injection, the gain in the outer region of the array is not fully utilized by the in-phase array mode. At certain injection levels, the unused gain may be sufficiently high to excite other higher order array modes. The highest order array mode has nulls in the optical field between each laser. Usually, the fundamental and highest order array modes have similar modal gains [26]. Therefore, the dominant array mode is determined by the amount of loss or gain in the interchannel regions [27]–[29]. If the cladding is lossy, the highest order array mode has the larger gain to oscillate as a main output beam due to its nulls in the interchannel regions.

The far-field pattern of each array mode of a 2×3 rectangular array is shown in Fig. 6. Fig. 6(a) and (b) show the far-field pattern along the x–z plane and the y–z plane, respectively. It is easily seen that Fig. 6(a) and (b) are the same as those of a two-element linear array and a three-element linear array of which amplitudes are modified by the interaction with each other.

The far-field pattern of the $N_1 \times N_2$ periodic array is just a multiplication of the N_1-element linear array along the x direction with the N_2-element linear array along the y direction as can be seen in (10). That is, the far-field pattern is the intersection of the two narrow main beams, plus those sidelobes from each conical pattern of the linear array which intersects with the conical main beam of the other linear array. Therefore, the fact that the fundamental mode has a single lobed far-field pattern and the highest order mode has a double lobed far-field pattern, which were observed in linear array, is also true in a two-dimensional periodic array as seen in Fig. 6(a) and (b).

We plotted the angular distribution of the output beam of 2×3 rectangular periodic array in which the center-to-center distance between lasers is 2 μm in Fig. 6(c). The outermost pattern and innermost pattern represent the an-

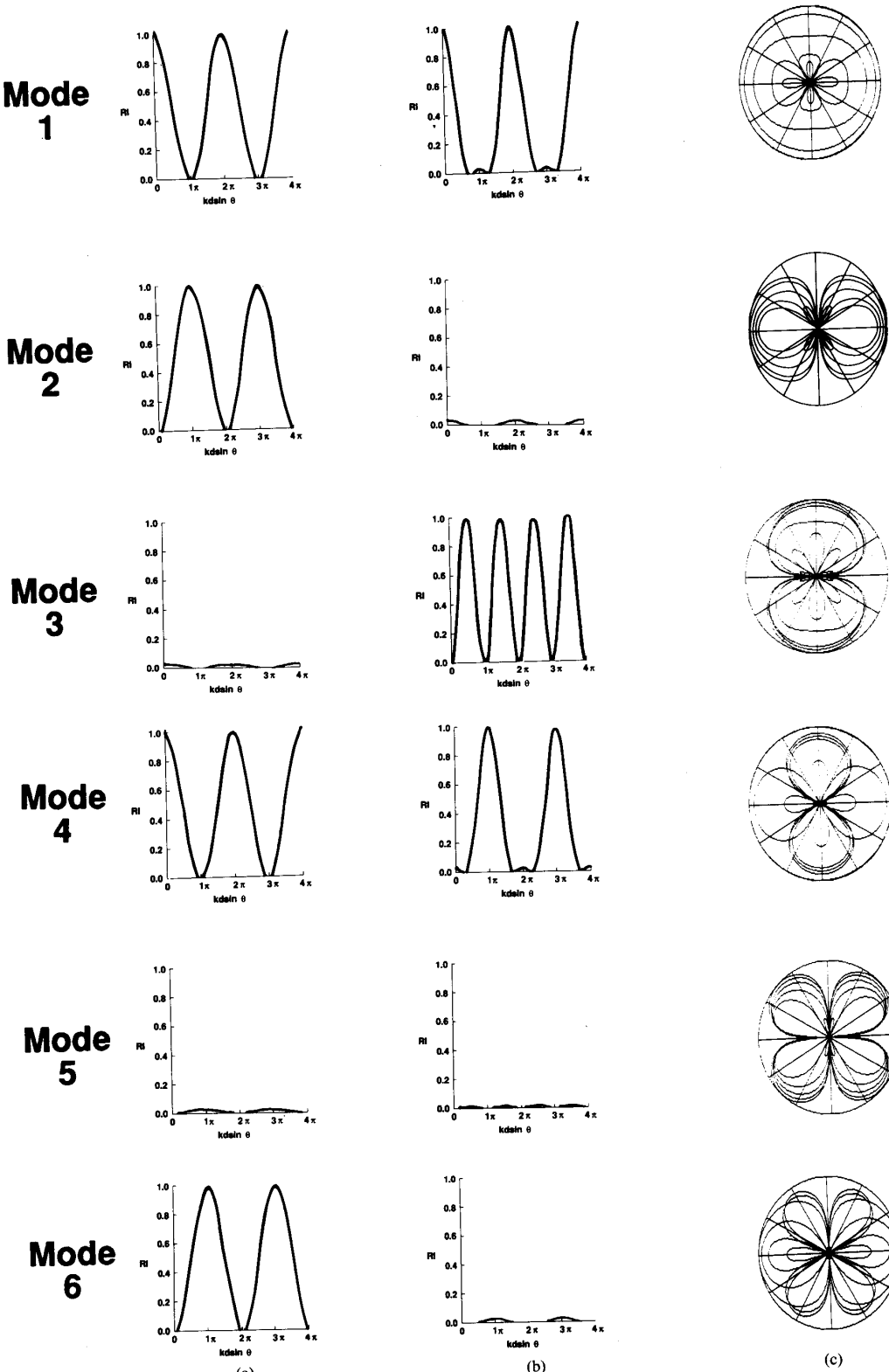

Fig. 6. Angular dependence of far-field patterns of 2 × 3 rectangular array. (a) Far-field distribution in x–z plane as a function of θ. (b) Far-field pattern in y–z plane as a function of θ. (c) Far-field distribution as function on ϕ, with θ as parameter. θ is in range of 0 to 16°.

gular distribution of the output beam at $\theta = 0°$ and $\theta = 16°$, respectively. Therefore, there are five patterns for $\theta = 0$, 4, 8, 12, and 16° in each circle of Fig. 6(c). For the convenience of illustration, their absolute magnitude has been changed and hence it is impossible to compare their relative amplitude out of this graph. We can observe that the two-dimensional array has a different angular distribution of the output beam at fixed θ and the angle of the field maximum is changed with the variation of θ. For example, for $p = 2$ and $q = 2$ (i.e., 5th-order array mode) in Fig. 6(c), the far-field pattern has its maxima along the off-axis of the array. In addition, with the increase of θ, more sidelobes become pronounced. If many of the array modes are excited, the beam divergence increases and the directionalty of the beam deteriorates because each mode has a different angular dependence.

B. Circular Array

The circular array in Fig. 3(b) is also called a ring array [22]. The only difference of this type of array from those of the linear array are its cyclic boundary condition. Similar structure has been analyzed for the longitudinal-coupled laser that has a mode selectivity using coupling between lasers [30]. If N-elements in the array, as shown in Fig. 7, support the same propagation constant, the coupled mode equation (3) becomes

$$\frac{dA_m}{dz} = iC_{mm+1}A_{m+1} + iC_{mm-1}A_{m-1}. \tag{11}$$

Assuming A_m has an $e^{i\delta mz}$ dependence, this equation can be written

$$\begin{bmatrix} -\delta_1 & C_{12} & 0 & 0 & \cdots & 0 & C_{1N} \\ C_{21} & -\delta_2 & C_{23} & 0 & \cdots & 0 & 0 \\ 0 & C_{32} & -\delta_3 & C_{34} & \cdots & 0 & 0 \\ \vdots & 0 & 0 & 0 & \cdots & 0 & 0 \\ 0 & & \cdots & & \cdots & -\delta_{N-1} & C_{N-1N} \\ C_{N1} & 0 & 0 & 0 & \cdots & -C_{NN-1} & -\delta_N \end{bmatrix} \cdot \begin{bmatrix} A_1 \\ A_2 \\ A_3 \\ \vdots \\ A_N \end{bmatrix} = 0. \tag{12}$$

This equation can be solved numerically. However, if the separation between each laser is equal to give the same amount of coupling between the nearest neighbor laser, the above equation can be simplified and easily solved as in Appendix A.

From (A.4),

$$\delta_m = -2C \cos(2\pi m/N) \tag{13}$$

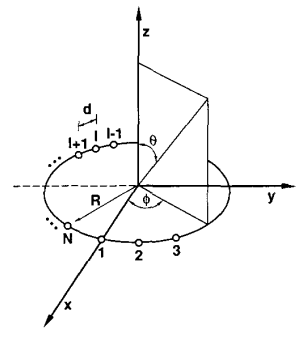

Fig. 7. N element circular array. Radius of array is R and each element is located on vertex of Nth polygon.

where $m = 1, 2, \cdots, N$. The propagation constant of the mth order array mode is given as

$$\gamma_m = \beta + C \cos(2\pi m/N). \tag{14}$$

Therefore, each array mode has a different propagation constant as is the case in the periodic array. Here again, the splitting in the propagation constant of the array mode is proportional to the coupling coefficient C. However, the range of the propagation constant is $\beta - 2C < \gamma < \beta + 2C$. Therefore, the maximum splitting of the longitudinal mode becomes $\Delta\lambda = 4C\lambda_0^2/2\pi n_e$ which is half of that for the periodic array. It implies that the circular array has a narrower spectrum and hence the possibility of having several array modes operating degenerately that is consistent with the results in [30].

The array factor of the mth order array mode is given as

$$AF_m(\theta, \phi) = \sum_{i=1}^{l=N} A_{lm} \exp\left[ik_0 R \sin\theta \cdot \cos(\phi - 2\pi l/N)\right]. \tag{15}$$

From (B.4), $A_{lm} = e^{i2\pi(m-1)l/N}$ and by substituting this equation into (15) the array factor of an N-element circular array can be obtained.

Fig. 8 is the schematic illustration of the near-field pattern of the six element circular array (or hexagonal array). Note that the fundamental mode has an equal amplitude of excitation across the array. Therefore, when each laser is pumped by uniform injection there is no unused gain unlike the case in the periodic array. We can observe that each supermode has a unique distribution of the saturated gain coefficient in each laser for a given injection level and a given total output intensity. As a result, the fundamental mode and highest mode have the highest possibility of lasing since every laser is equally excited. As is the case with the periodic array, the mode discrimination comes from the amount of loss or gain in the interchannel region. If the cladding is lossy, the highest order array mode would have the lowest threshold since the unpumped region corresponds to an area of small modal intensity.

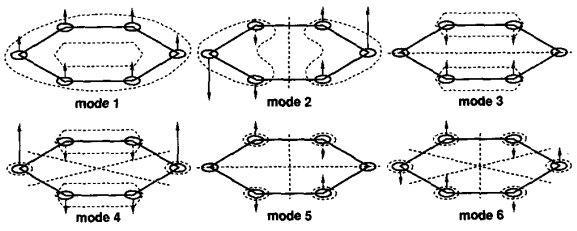

Fig. 8. Schematic illustration of near-field distribution of supermodes across six-element circular array (or hexagonal array).

Fig. 9 shows the normalized far-field intensity distribution for the array modes of a hexagonal array of radius 3 μm. It is interesting to note that Fig. 9 and Fig. 6 have many features in common. The direction of field nulls and maxima are very similar to each other. However, we can observe that Fig. 9(c) has more circular symmetry. Fig. 9(a) and (b) are the far-field pattern of the hexagonal array along the x–z plane and the y–z plane, respectively. Note that the x and y direction are not always the direction for maximum field. Fig. 9(c) shows the azimuthal angle dependence of the circular array for various values of θ. Each circle has five patterns at $\theta = 0$, 4, 8, 12, and 16°. The outermost pattern is at $\theta = 0°$ and inner most pattern is at 16°. Each pattern is normalized and hence it is impossible to compare their relative magnitudes out of this picture as in the case of Fig. 6(c). The fundamental mode has a single center lobe near zenith, and with increasing θ, six field maxima appear along the symmetric axis of the array. The highest order mode has a six field maxima near the zenith and with increase of θ, 12 field maxima appear which give a wider far-field beam divergence. If there are some nonlinearities such as nonuniform active layer thickness or nonuniform current injection, several array modes oscillate together giving a wide modal spectrum and beam divergence.

C. Centered Polygonal Array

The centered polygonal array, shown in Fig. 3(c), may be called a concentric circular array [23], which can be considered to be the centered polygonal array with the addition of a center laser. This array structure has been analyzed and fabricated using optical fibers for the wavelength-insensitive mode coupler applications [31], [32]. This array is particularly interesting for understanding the effect of the center laser on the resulting supermodes. In addition, the physical understanding can be extended to the analysis of more complicated concentric circular arrays.

The coupled mode equation can be simplified by the nearest-neighbor coupling approximation. In this case, each of the outer N lasers couples equally to its two neighbors in addition to the coupling to the center laser. As can be easily understood from Fig. 3(c) and the following analysis, the coupling between the center laser and the outer laser should occur between different propagation constants. Taking the mode difference into considerations, we get the coupled mode equation (3) as

$$\sum_{l=1}^{N} \frac{dA_l}{dz} = 2iC \sum_{l=1}^{N} A_l + \sum_{l=1}^{N} iC' A_0 e^{i(\beta_0 - \beta_l)z} \quad (16)$$

$$\frac{dA_0}{dz} = iC' \sum_{l=1}^{N} A_l e^{i(\beta_l - \beta_0)z} \quad (17)$$

where C is the coupling coefficient between the two outer lasers and C' is the coupling coefficient between the center laser and an outer laser.

By making the substitutions,

$$\Pi_1(z) = A_0(z) \quad (18)$$

$$\Pi_2(2) = \frac{1}{\sqrt{N}} \sum_{l=1}^{N} A_l(z) \exp(-iCz) \quad (19)$$

and $\beta_0 - \beta = \Delta$, where $\beta = \beta_1 = , \cdots , = \beta_N$, we can reduce the coupled mode equation of the centered polygon array to a simple two mode problem as shown in Fig. 10. That is

$$\frac{d\Pi_2}{dz} = i\sqrt{N}C' e^{i\Delta z}\Pi_1 \quad (20)$$

$$\frac{d\Pi_1}{dz} = i\sqrt{N}C' e^{i\Delta z}\Pi_2. \quad (21)$$

Therefore, we can get the array mode propagation constant as follows:

$$\gamma = \frac{\beta_0 + \beta - 2C}{2} \pm \sqrt{\Delta^2 + NC'2}. \quad (22)$$

The "+" and "−" are for the propagation constant of the even mode and odd mode as shown in Fig. 10. Note that the splitting in mode propagation constant between even and odd modes becomes large with the increase of N. From the symmetry of the structure, it can be easily shown that the high-order array modes of a centered polygonal array are the same as those of a circular array of N-elements.

Fig. 11 shows a schematic of the near-field intensity distribution of the centered hexagonal array. Compared with Fig. 8 the high-order array modes have the same near-field intensity distribution as the hexagonal array. The first mode is the even mode and the second mode is the odd mode. Note that the in-phase array mode has a field amplitude distribution peaked on the center laser. As is the case for the periodic array, the gain of the laser in the outer ring of the array is not fully utilized by the in-phase array mode. At a certain injection level, the unused gain may be sufficiently high to support other higher array modes. One interesting observation in the case of the centered polygonal array is that the first- and second-order array modes are the possible oscillation modes. Since the higher array modes do not excite the center laser, it is difficult for this to occur under uniform current injection conditions. The modal discrimination comes from the amount of loss or gain in the region between the ring and center laser. If the cladding is lossy, the second-order ar-

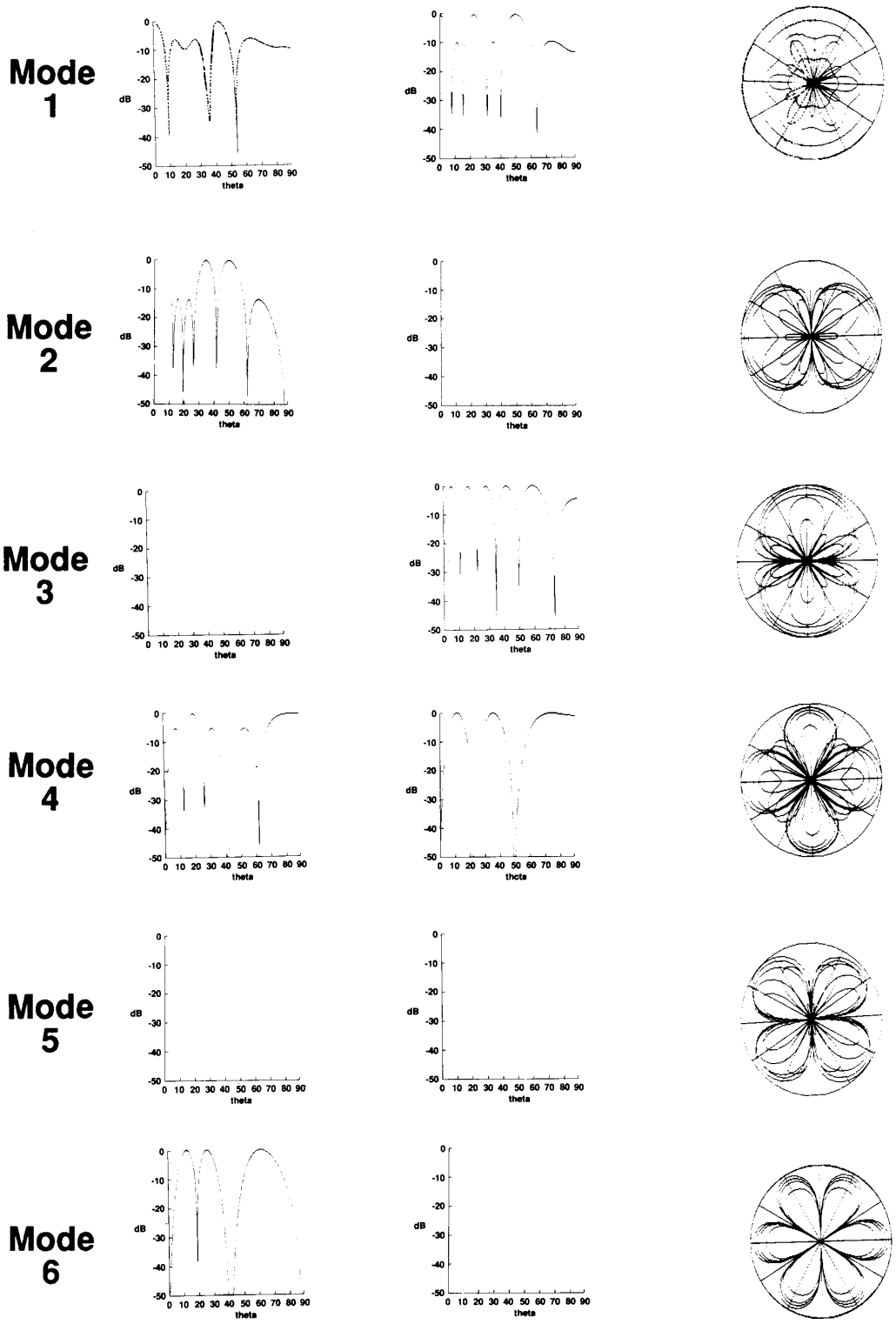

(a) (b) (c)

Fig. 9. Angular dependence of far-field patterns of six-element circular array. (a) and (b) Far-field distribution as function of θ in x–z plane and y–z plane, respectively. (c) Far-field distribution as function of ϕ with θ as parameter. θ is in range of 0 to 16°.

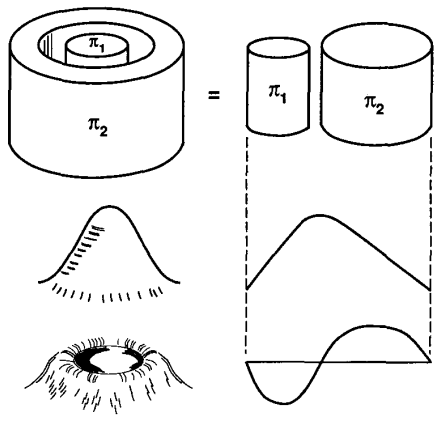

Fig. 10. Two-channel coupled waveguide.

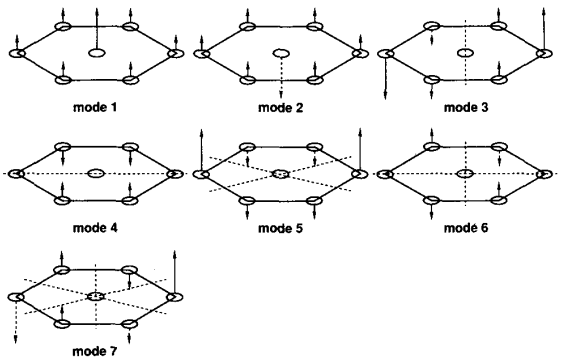

Fig. 11. Schematic illustration of near-field distribution of supermodes across a centered hexagonal array.

ray mode would have the lowest threshold since the unpumped region corresponds to a field null.

The far-field pattern of the array modes of a centered polygonal array are the same as those of the circular array for the higher order array modes. For the first- and second-order array modes, the array factors are given as

$$AF_m(\theta, \phi) = AF_{\text{circular}} + B_m = \sum_{l=1}^{N} A_{lm} \exp\left[ik_0 R \sin\theta \cdot \cos(\phi - 2\pi l/N)\right] + B_m \quad (23)$$

where

$$B_m = \pm \frac{\sqrt{\Delta^2 + NC'^2} - \Delta}{\sqrt{NC'}}$$

where "+" and "−" are for $m = 1$ and 2, respectively. The effect of the addition of B_m is to neutralize the sidelobes of the beam pattern, as seen in Fig. 12, which shows the far-field pattern of the first- and second-order array modes of the centered hexagonal array for various values of excitation amplitudes of the center laser. The far-field pattern of the remaining higher order array modes is similar to that of the hexagonal array and is omitted here. The difference in the far-field pattern between the first- and second-order array modes is that the first mode has less pronounced sidelobes at large θ and the second mode has more pronounced sidelobes at large θ, as seen in Fig. 12. As can also be seen in Fig. 12, the beam pattern can be made more symmetric by increasing the excitation amplitude of the center laser.

IV. Discussion

From the previous analysis, it can be seen that the symmetry and periodicity of the array structure plays an important role in determining the array mode of a planar array. The symmetry gives a finite phase relationship among elementary lasers of the array leading to an array mode. The lowest order mode is the most symmetric and highest array mode is the least symmetric as easily seen in Fig. 5, 8 and 11. We have shown that the analysis can be made easy by using the symmetry operations as outlined in Appendix B. For the lossy cladding the highest order array mode lases easily, except in the case of the centered polygonal array, since it has the optimum overlap of the electron distribution and the optical field distribution leading to a wide beam divergence, which was observed in linear array experiment [33]. This can be avoided if we reduce the loss in the interchannel region by insertion of net gain in the interchannel region [28], [29].

When ϕ symmetry (azimuthal angular symmetry) of the output beam pattern is important, the circular array fits the symmetry requirement. The periodic array has a relatively poor ϕ-symmetry as shown in Fig. 6. The sidelobes along the off axis are the result of the intersection of a conical sidelobe of the x directed linear array with a conical sidelobe of the y directed linear array. The reduction of these sidelobes results to the broad beamwidth of the far-field pattern [24]. But as we can see in Fig. 9, the particular example of hexagonal array is not likely to have a superior ϕ-symmetry. However, if we increase the number of elements in a circular array, the array pattern approaches that of a continuous ring to give a $J_1(k_0 R \sin\theta)/k_0 R \sin\theta$ beam pattern which has no ϕ-dependence [24]. This case is also true for the centered polygonal array. Based on the results of analysis of the circular array and centered polygonal array, we can derive the beam pattern of the more complicated concentric circular array as just the superposition of the array factor of each circular array [23]. By using this concentric circular array, we can make the beam pattern more circular (better ϕ symmetry). In addition, we can understand that a more symmetric beam pattern can be realized by forcing only the fundamental mode to oscillate by proper design, such as the variation of the distance between each ring (varying the coupling coefficient) [34] or variation of the laser radius in a different ring [35], as shown in Fig. 13. For example, if the lasers in the rings near the center have a larger radius than lasers in outer rings, such as in a chirped array [35], the gain distribution across the array prefers to support a single circular output beam as the fundamental mode.

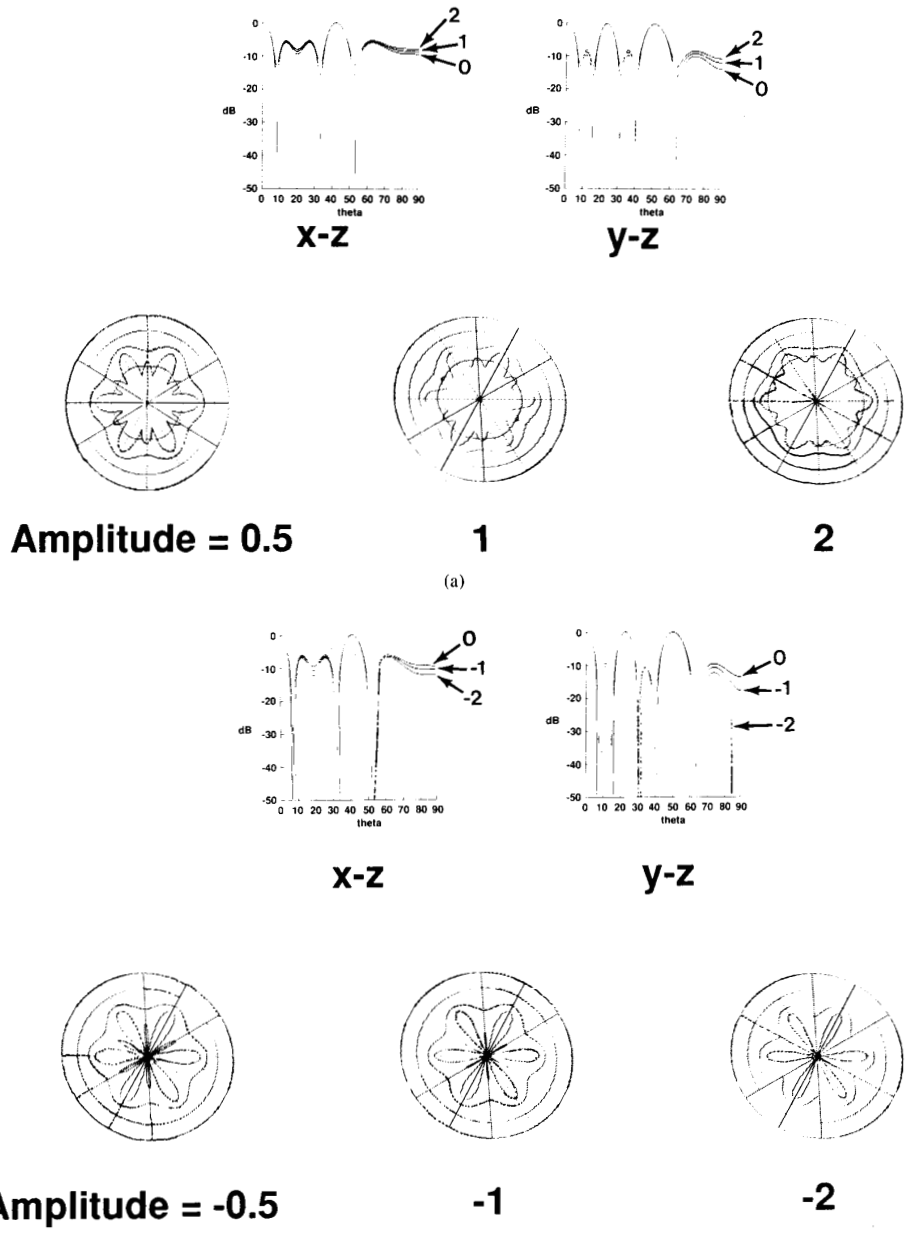

Fig. 12. Far-field distribution of centered hexagonal array. (a) and (b) Far-field pattern for various excitation amplitudes of center laser for first- and second-order supermode, respectively.

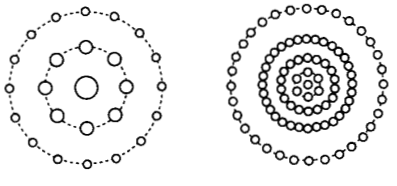

(a) (b)

Fig. 13. Schematic diagram for modified array structure for obtaining circular symmetric far-field pattern. (a) Chirped array. (b) Variable spacing array.

With an array covering a much wider active area than a linear array, it is expected that any compositional nonuniformity or any nonuniform current injection is likely to cause a corresponding broadening in the spectral gain profile. Therefore, the two-dimensional array is more likely to lase with multiple longitudinal modes than a linear array. Since the VCSE laser has a very short cavity length, the mode spacing can be very large [12]. The DBR-high reflectance mirror, which the VCSE laser has, also shows the mode selectivity [36]. In addition, its ac-

tive layer is a thin quantum well which gives a narrower gain spectrum [37]. These properties may bring mode stability to a two-dimensional VCSE laser array such that even dynamic single-mode operation can be achieved [38].

For a pure array mode to occur, a given phase relationship must be maintained from the reflection at the laser facet. If there are imperfections in the mirror, extra relative phase shifts will be introduced in the reflected beam of each laser. Under this condition, array modes are coupled to give an admixture of array modes to satisfy the lasing condition which brings about a broad beam divergence [39]. However, the VCSE laser has a multiple quarter wavelength AlAs–GaAs layers, which are precisely grown by MBE, for distributed reflection achieving very high reflectance of more than 99% and hence negligible imperfections [40] the admixture of array modes due to mirror imperfections can be avoided. In contrast, we can bring artificial mirror imperfections to the mirror reflectivity distribution across the array simply changing the number of AlAs–GaAs layers. This can be done using a conventional etching process. That is, we can control not only the phase of each laser but also the far-field beam pattern of the two-dimensional array using a simple etching process.

One interesting application of the result of the two-dimensional array analysis is the design of a quantum box laser array. If we reduce the diameter of the VCSE laser to several hundred angstroms, each laser behaves as a quantum box laser [41]. These structures have potential advantages such as reduced threshold current density, improved field spectrum linewidth and improved temperature dependence [42]. Usually the quantum box laser has an array structure for the efficient interaction between the optical mode and closely confined electrons. As in the previous analysis, the optical field distribution has a peak in the middle of the array and in the outer region the optical gain is not fully utilized under uniform current injection. This excess gain may bring spectral instability to an array of quantum box lasers. Therefore, we can apply the previous results to bring mode stability such as varying the distance between the quantum boxes or varying the size of the quantum box.

V. Conclusion

We have investigated the properties of a two-dimensional array of vertical cavity surface emitting lasers. The evanescent coupling between VCSE lasers brings spatial coherence across the array aperture for phase locking between lasers. Since the VCSE laser has a very short cavity length, the longitudinal mode spacing can be very large. Also, the VCSE laser has a quantum-well active layer that has a narrow spectral gain. Therefore, the two-dimensional array comprising of VCSE laser has good modal selectivity that can achieve dynamic single-mode operation. The coupling between two VCSE lasers depends on the radius of the lasers, distance between lasers and the surrounding medium. A larger coupling coefficient is obtained due to the farther penetration of the field into the cladding with the decrease of the laser radius and increase of the cladding refractive index.

Typical two-dimensional arrays are a periodic array, a circular array and a centered polygonal array (or concentric array). When there exists a finite coupling between lasers, the optical mode of the array can be represented by the superposition of array modes. Each mode has its characteristic near-field distribution across the array and a different propagation constant. We found that for the same number of elements the maximum splitting of the propagation constants of the array modes of the periodic array is twice that of the circular array. The near-field pattern of the array mode suggests that the fundamental mode and highest array mode have the highest possibility of lasing under uniform current injection conditions. In addition, the mode discrimination between the fundamental mode and highest mode comes from the amount of loss or gain in the interchannel region. If the cladding is lossy, the highest array mode of the periodic array or circular array and the second order array mode of the centered polygonal array would have the lowest threshold. In a two-dimensional array, the field maximum of the far-field pattern has an azimuthal angle dependence. The fundamental mode has a single center lobe near the zenith. But with the increase of θ it has several field maxima. The circular array and centered polygonal array have better ϕ-symmetry in the far-field pattern. Also, the centered polygonal array has a more circularly symmetric beam pattern that can be controlled by varying the excitation amplitude of the center laser. Single-mode operation can come from the reduction of loss in the interchannel region, varying the distance between lasers (varying the coupling coefficient) or varying the radius of the lasers, as in the case of the linear array.

The symmetry of an array structure in two dimensions plays an important role in determining the array modes. Also, the beam broadening due to imperfections in the mirror can be avoided in VCSE lasers since precisely controlled epi-growth by MBE is used. Alternatively, we can control the mirror imperfections by simply etching to introduce phase changes among the elementary lasers. If the radius of the lasers reduces to the quantum limit, each laser behaves as a quantum box laser. The results of the above analysis can be employed in the control of the mode characteristics of the quantum box laser arrays to bring a single mode operation.

Appendix A

Since every coupling coefficient is the same, (5) becomes

$$\begin{bmatrix} x & 1 & 0 & 0 & \cdots & 1 \\ 1 & x & 1 & 0 & \cdots & 0 \\ 0 & 1 & x & 1 & \cdots & 0 \\ 0 & 0 & 1 & x & \cdots & \vdots \\ \vdots & & & & \cdots & 1 \\ 1 & 0 & 0 & 0 & \cdots & x \end{bmatrix} \begin{bmatrix} A_1 \\ A_2 \\ A_3 \\ A_4 \\ \vdots \\ A_N \end{bmatrix} = 0 \tag{A1}$$

where $x = -\delta/c$. For the existence of nontrivial solution, its determinant must be zero. Since it is an nth order cyclic determinant, it becomes nth order x equation such as

$$\prod_{l=1}^{N} (x + e^{2\pi il/N} + e^{-2\pi il/N}) = 0. \quad \text{(A2)}$$

Therefore, the solution is given by

$$x = -2 \cos (2\pi l/N),\ l = 1, 2, \cdots, N \quad \text{(A3)}$$

and the δ is given as

$$\delta = -2C \cos (2\pi l/N). \quad \text{(A4)}$$

Appendix B

If the array has a rotational symmetry by $2\pi/N$ rotation, its array mode has O_{C_N} symmetry where O_{C_N} is the symmetry operator such as

$$O_{C_N}\psi_l = e^{2\pi lk/N}\psi_L \qquad k = 0, 1, \cdots, N-1 \quad \text{(B1)}$$

$$\sum_{m=1}^{N} A_{lm} O_{C_N} E_m = \sum_{m=1}^{N} A_{lm} e^{2\pi ik/N} E_m$$

$$\sum_{m=1}^{N} A_{lm} E_{m-1} = \sum_{m=1}^{N} A_{lm} e^{2\pi ik/N} E_m$$

$$\sum_{m=1}^{N} A_{lm+1} E_m = \sum_{m=1}^{N} A_{lm} e^{2\pi ik/N} E_m \quad \text{(B.2)}$$

where $E_o = E_N$ and $A_{lN+1} = A_{l1}$. Therefore, we can get the relationship between A_{lm+1} and A_{lm} as

$$A_{lm+1} = A_{lm} e^{2\pi ik/N}. \quad \text{(B3)}$$

If we choose $A_{l1} = 1$,

$$A_{lm} = \exp [2\pi lk(m-1)/N],$$
$$k = 0, 1, \cdots, N-1. \quad \text{(B4)}$$

If array modes are degenerate, we can remove the degeneracy by superposition of the array modes. For example, in a hexagonal array the second- and third-order array modes are degenerate and the fourth- and fifth-order modes are degenerate. Therefore, we choose second- (or fourth-) order mode as the summation of two modes and third- (or fifth-) order mode as the difference of the two modes such as

$$\psi_2' = (\psi_2 + \psi_3)/2,\ \psi_3' = (\psi_2 - \psi_3)/2 \quad \text{(B5)}$$

$$\psi_4' = (\psi_4 + \psi_5)/2,\ \psi_5' = (\psi_4 - \psi_5)/2 \quad \text{(B6)}$$

Acknowledgment

The authors would like to thank Dr. Y. H. Lee of AT&T for helpful discussions. In addition, gratitude is extended to Dr. T.-K. Yoo of Gold Star Central Research Institute and Dr. J. Woong of the Kukje Semiconductor Co. for their deep interests in this research.

References

[1] D. R. Scifres, C. Lindstrom, R. D. Burnham, W. Streifer, and T. L. Paoli, "Phase-locked (GaAl)As laser diode emitting 2.6 W CW from a single mirror," *Electron. Lett.*, vol. 19, pp. 169-170, 1983.

[2] G. L. Harnagel, D. R. Scifres, H. H. Kung, D. F. Welch, D. P. Worland, P. S. Cross, and R. D. Burnham, "Five watt continuous GaAlAs laser diodes," *Electron. Lett.*, vol. 22, pp. 605-606, 1986.

[3] G. A. Evans, N. W. Carlson, J. M. Hammer, M. Lurie, J. K. Butler, S. L. Palfrey, R. Amantea, L. A. Carr, F. Z. Hawrylo, E. A. Janes, C. J. Kaiser, J. B. Kirk, W. F. Reichert, S. R. Chinn, J. R. Shearly, and P. S. Zory, "Coherent, monolithic two-dimensional (10 × 10) laser arrays using grating surface emission," *Appl. Phys. Lett.*, vol. 53, pp. 2123-2125, Nov. 1988.

[4] J. J. Yang, L. Lee, M. Jansen, M. Sergent, S. S. Ou, and J. Wilcox, "Monolithic two-dimensional surface emitting arrays of GaAs/AlGaAs lasers," *Fiber Integrat. Opt.*, vol. 7, pp. 217-228, 1988.

[5] Z. L. Liau and J. N. Walpole, "Large monolithic two-dimensional arrays of GaInAsP/InP surface-emitting lasers," presented at Top. Meet. on Semicond. Lasers, Feb. 1987, (IEEE LEOS and Opt. Soc. Amer., Albuquerque, NM,) paper WA2, pp. 84-86.

[6] J. Buus, P. J. Williams, I. Goodridge, D. J. Robbins, J. Urquhart, A. P. Webb, T. Reid, R. Nicklin, P. Charles, D. C. J. Reid, and A. C. Carter, "Surface-emitting two-dimensional coherent semiconductor laser array," *Appl. Phys. Lett.*, vol. 55, pp. 331-333, 1989.

[7] F. Koyoma, S. Kinoshita, and K. Iga, "Room temperature cw vertical cavity surface emitting laser and high power 2-D laser array," in *Tech. Dig., CLEO'89.* Baltimore, MD: Opt. Soc. Amer., paper FC1.

[8] D. P. Bour, P. Stabile, A. Rosen, W. Jonton, L. Elbaum, and D. J. Holmes, "Two-dimensional array of high power strained quantum well lasers with $\lambda = 0.95$ μm," *Appl. Phys. Lett.*, vol. 54, pp. 2637-2638, 1989.

[9] S. L. McCall, A. C. Gossard, J. H. English, J. L. Jewell, Y. H. Lee, and A. Scherer, "Lasing monolithic microresonator arrays," *Appl. Phys. Lett.*, vol. 51, pp. 94-96, 1987.

[10] H.-J. Yoo, A. Scherer, J. P. Harbison, L. T. Florez, E. G. Pack, B. P. Van der Gaag, J. R. Hayes, A. Von Lehmen, E. Kapon, and Y.-S. Kwon, "Fabrication of a two-dimensional phased array of vertical-cavity surface-emitting lasers," *Appl. Phys. Lett.*, vol. 56, pp. 1198-1200, Mar. 1990.

[11] J. K. Butler, D. E. Ackley, and D. Botez, "Coupled-mode analysis of phase-locked injection laser arrays," *Appl. Phys. Lett.*, vol. 44, pp. 293-295, Feb. 1984.

[12] K. Iga, F. Koyama and S. Kinoshita, "Surface emitting semiconductor lasers," *IEEE J. Quantum Electron.*, vol. 24, pp. 1845-1855, Sept. 1988.

[13] J. L. Jewell, A. Scherer, S. L. McCall, Y. H. Lee, S. J. Walker, J. P. Harbinson, and L. T. Florez, "Low threshold electrically-pumped vertical-cavity surface-emitting micro-lasers," *Electron. Lett.*, vol. 25, pp. 1123-1124, 1989.

[14] A. Ibaraki, K.Kawashima, K. Furusawa, T. Ishikawa, T. Yamaguchi, and T. Niina, "Buried heterostructure GaAs/AlAs distributed Bragg reflector surface emitting laser with very low threshold (5.2 mA) under room temperature CW condition," *Japan. J. Appl. Phys.*, vol. 28, pp. L667-668, Apr. 1989.

[15] L. M. Zinkiwicz, T. J. Roth, L. J. Mawst, D. Tran, and D. Botez, "High-power vertical-cavity surface-cavity surface-emitting AlGaAs/GaAs diode lasers," *Appl. Phys. Lett.*, vol. 54, pp. 1959-1961, May 1989.

[16] M. Ogura, W. Hsin, M.C. Wu, S. Wang, and J. R. Whinnery, "Surface-emitting laser diode with vertical GaAs/GaAlAs quarter-wavelength multilayers and lateral buried heterostructure," *Appl. Phys. Lett.*, vol. 51, pp. 1655-1657, Nov. 1987.

[17] *Light Transmission Optics*, D. Marcuse, New York: Van Nostrand Reinhold, 1982.

[18] H.-J. Yoo, J. R. Hayes, and Y. S. Kwon, "Analysis of coupling loss between two vertical cavity lasers," to be published.

[19] R. Vanclooster and P. Phariseau, "The coupling of two parallel dielectric fibers, Part II," *Physica*, vol. 47, pp. 501-514, 1970.

[20] J. K. Butler, D. E. Ackley, and M. Ettenberg, "Coupled-mode analysis of gain and wavelength oscillation characteristics of diode laser phased arrays," *IEEE J. Quantum Electron.*, vol. QE-21, pp. 458-464, May 1985.

[21] L. Stark, "Microwave theory of phased-array antennas—A review," *Proc. IEEE* vol. 62, pp. 1661-1701, Dec. 1974.

[22] W. R. Lepage, C. S. Roys, and S. Seely, "Radiation from circular current sheets," *Proc. IRE*, pp. 1069-1072, Sept. 1950.

[23] C. O. Stearns and A. C. Stewart, "An investigation of concentric ring antennas with low sidelobes," *IEEE Trans. Ant. Prop.* vol. AP-13, pp. 856-863, Nov. 1965.

[24] See the microwave antenna theory text for example, R. S. Elliot, *Antenna Theory and Design.* Englewood Cliffs, NJ: Prentice-Hall,

1981 or M. T. Ma, *Theory and Application of Antenna Array*. New York: Wiley, 1974.
[25] *Introduction to Solid State Physics*, 5th ed., C. Kittel, Ed. New York: Wiley, 1976, ch. 1.
[26] E. Kapon, "The supermode structure of phase-locked diode laser arrays with variable channel spacing," *IEEE J. Quantum Electron.*, vol. QE-23, pp. 89-93, Jan. 1987.
[27] D. Botez and J. C. Connolly, "High-power phase-locked array of index-guided diode lasers," *Appl. Phys. Lett.*, vol. 43, pp. 1096-1098, Dec. 1983.
[28] D. R. Scifres, R. D. Burnham, and W. Streifer, "Lateral grating array high power CW visible semiconductor laser," *Electron Lett.*, vol. 18, pp. 549-550, Jun. 1982.
[29] S. Mukai, C. Lindsey, J. Katz, E. Kapon, Z. Rav-Noy, S. Margalit, and A. Yariv, "Fundamental mode oscillation of a buried-ridge waveguide laser array," *Appl. Phys. Lett.*, vol. 45, pp. 834-835, 1984.
[30] W. J. Fadar and G. E. Palma, "Normal modes of N coupled lasers," *Opt. Lett.*, vol. 10, no. 8, pp. 381-383, 1985.
[31] A. W. Snyder, "Coupled-mode theory for optical fibers," *J. Opt. Soc. Amer.*, vol. 62, no. 11, pp. 1267-1277, 1972.
[32] D. B. Mortimore and J. W. Arkwright, "Monolithic wavelength-flattened 1 × 7 single mode fused coupler," *Electron Lett.*, vol. 25, pp. 606-607, 1989.
[33] D. R. Scifres, R. D. Burnham, C. Lindstrom, W. Streifer, and T. L. Paoli, "Phase-locked (GaAl)As laser emitting 1.5W CW per mirror," *Appl. Phys. Lett.*, vol. 42, pp. 645-647, 1983.
[34] D. E. Ackley, J. K. Butler, and M. Ettenberg, "Phase-locked injection laser arrays with variable stripe spacing," *IEEE J. Quantum Electron.*, vol. QE-22, pp. 2204-2212, Dec. 1986.
[35] E. Kapon, C. P. Lindsey, J. Katz, S. Margalit, and A. Yariv, "Chirped arrays of diode lasers for supermode control," *Appl. Phys. Lett.*, vol. 45, pp. 200-202, 1984.
[36] Y. Suematsu, S. Arai, and K. Kishino, "Dynamic single mode semiconductor laser with a distributed reflector," *J. Lightwave Technol.*, vol. LT-1, pp. 161-176, 1983.
[37] N. Holonyak, Jr., R. M. Kolbas, R. D. Dupuis, and P.D. Dapkus, "Quantum-well heterostructure lasers," *IEEE J. Quantum Electron.*, vol. QE-16, pp. 170-186, Feb. 1980.
[38] H. Soda, Y. Motegi, and K. Iga, "GaInAsP/InP surface emitting injection lasers with very short cavity length," *IEEE J. Quantum Electron.*, vol. QE-19, pp. 1035-1041, June 1984.
[39] K. L. Chen and S. Wang, "Effect of mirror imperfections on phase-locked semiconductor laser arrays," *IEEE J. Quantum Electron.*, vol. QE-21, pp. 264-270.
[40] Y. H. Lee, private communication.
[41] Y. Arakawa and H. Sasaki, "Multidimensional quantum well laser and temperature dependence of its threshold current," *Appl. Phys. Lett.*, vol. 40, pp. 939-941, June 1982.
[42] K. J. Vahala, "Quantum box fabrication tolerance and size limits in semiconductors and their effect on optical gain," *IEEE J. Quantum Electron.*, vol. 24, pp. 523-530, Mar. 1988.

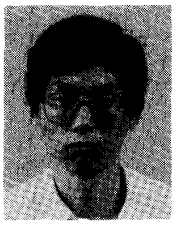

Hoi-Jun Yoo was born in GongJu, ChungNam, Korea, on July 30, 1960. He received the B.S. degree in electronic engineering from Seoul National University in 1983, and the M.S. and Ph.D. degrees in electrical engineering from the Korea Advanced Institute of Science and Technology (KAIST), in 1985 and 1988, respectively.

In 1988, he joined the Department of Electrical Engineering, KAIST as a Postdoctoral Researcher and studied on the GaAs-AlGaAs laser diodes, heterojunction bipolar transistors, and vertical integration of optoelectronic devices. Since September 1988, he has been with Bellcore as a Visiting Researcher and his interests have been the InP-InGaAs HBT and vertical cavity surface emitting lasers. He is an inventor of the InP-InGaAs lateral HBT and Front Surface Emitting Laser Diode (FSELD).

J. R. Hayes (M'89), photograph and biography not available at the time of publication.

Eung Gi Paek received the B.Sc. degree in physics from Seoul National University in 1972 and the M.Sc. and Ph.D. degrees in physics from the Korea Advanced Institute of Science and Technology in 1976 and 1979, respectively.

From 1979 to 1981, he worked at the Agency for Defense Development in Korea. In April 1982, he joined the California Institute of Technology, Pasadena, as a Postdoctoral Fellow and later as a Senior Research Fellow for a period of five years. Since May 1987, he has been with Bell Communications Research as a member of the technical staff. His current research interests are in the areas of optical implementations of neural network models, hybrid optical signal-image processing, and pattern recognition using semiconductor devices.

A. Scherer, photograph and biography not available at the time of publication.

Young-Se Kwon received the B.S. degree from Seoul National University in 1968, the M.S. degree from Ohio State University, Columbus, in 1972, and the Ph.D. degree in electrical engineering from University of California, Berkeley in 1977.

From 1977 to 1979, he was a Research Associate at Department of Electrical Engineering, Duke University, Durham, NC. In June 1979, he joined the Department of Electrical Engineering, Korea Advanced Institute of Science and Technology as an Assistant Professor, and in 1988 he became a Full Professor. Since 1979, he has studied on integrated optics, laser diodes, high speed transistors, and optoelectronic integrated circuits. He is an author and coauthor of more than 60 technical papers.

Prof. Kwon is a member of the Korea Institute of Electronic Engineers and the American Institute of Physics.